npj | systems biology and applications

Article

Published in partnership with the Systems Biology Institute

https://doi.org/10.1038/s41540-024-00433-6

Multistability and predominant hybrid phenotypes in a four node mutually repressive network of Th1/Th2/Th17/Treg differentiation

Atchuta Srinivas Duddu[1], Elizabeth Andreas[2], Harshavardhan BV[1,3], Kaushal Grover[4], Vivek Raj Singh[5], Kishore Hari[1,6,7], Siddharth Jhunjhunwala[1], Breschine Cummins[2] ✉, Tomas Gedeon[2] ✉ & Mohit Kumar Jolly[1] ✉

Elucidating the emergent dynamics of cellular differentiation networks is crucial to understanding cell-fate decisions. Toggle switch – a network of mutually repressive lineage-specific transcription factors A and B – enables two phenotypes from a common progenitor: (high A, low B) and (low A, high B). However, the dynamics of networks enabling differentiation of more than two phenotypes from a progenitor cell has not been well-studied. Here, we investigate the dynamics of a four-node network A, B, C, and D inhibiting each other, forming a toggle tetrahedron. Our simulations show that this network is multistable and predominantly allows for the co-existence of six hybrid phenotypes where two of the nodes are expressed relatively high as compared to the remaining two, for instance (high A, high B, low C, low D). Finally, we apply our results to understand naïve CD4$^+$ T cell differentiation into Th1, Th2, Th17 and Treg subsets, suggesting Th1/Th2/Th17/Treg decision-making to be a two-step process.

Multistability—the co-existence of more than one steady state/phenotype—is a hallmark of gene regulatory networks (GRNs) driving cellular differentiation and reprogramming. It is the defining trait of a switch that allows the ability to achieve multiple states without altering internal genetic content[1,2]. Thus, decoding the emergent dynamics of underlying regulatory networks is crucial for mapping the cell-fate trajectories. Toggle switch—a mutually inhibitory feedback loop between two nodes—is a bistable network motif. A toggle switch between two master regulators, A and B, often leads to the co-existence of two mutually exclusive cell-states—(low A, high B) and (high A, low B)[3,4]. This feature makes it suitable for investigating the differentiation of a precursor cell into two sister lineages. However, the emergent dynamics of GRNs involved in the differentiation of a common progenitor into more than three phenotypes have not yet been as well-studied.

CD4 + T-cells offer an intriguing model system to investigate multistable dynamics with plasticity seen among multiple CD4 + T-cell subsets both in vitro and in vivo—Th1, Th2, Th9, Th17 and Treg. Specific cytokines can polarize naïve CD4 + T-cells towards these different subsets. Each T-cell subset has unique cytokine production and immune function profile, and retains the capacity to reprogram to other cell-states when exposed to different cytokine environments[5]. The lineage-specifying transcription factors corresponding to Th1, Th2, and Th17 – T-bet, GATA3 and RORγT – have been shown to repress each other, thus forming a toggle triad[6]. Our previous work showed that a toggle triad between A, B and C can enable the co-existence of three differentiated states – (high A, low B, low C), (low A, high B, low C) and (low A, low B, high C) and switching among them. Moreover, three hybrid or 'double-positive' states – (high A, high B, low C), (low A, high B, high C) and (high A, low B, high C) were also observed, albeit at a lower frequency than the differentiated ones. These results could explain the experimentally observed phenotypic switching among Th1 (high T-bet, low GATA3, low RORγT), Th2 (low T-bet, high GATA3, low RORγT), Th17 (low T-bet, low GATA3, high RORγT), and the hybrid Th1/Th2, Th1/Th17 and Th2/Th17 states[7,8].

[1]Department of Bioengineering, Indian Institute of Science, Bangalore, 560012, India. [2]Department of Mathematical Sciences, Montana State University, Bozeman, MT, 59717, USA. [3] IISc Mathematics Initiative, Indian Institute of Science, 560012 Bangalore, India. [4]School of Computational and Integrative Sciences, Jawaharlal Nehru University, New Delhi, 110067, India. [5]Undergraduate Program, Indian Institute of Science, Bangalore, 560012, India. [6] Department of Physics, Northeastern University, MA, 02115 Boston, USA. [7]Present address: Center for Theoretical Biological Physics, Northeastern University, MA, 02115 Boston, USA.
✉e-mail: breschine.cummins@montana.edu; tgedeon@montana.edu; mkjolly@iisc.ac.in

Besides the Th1/Th2/Th17 toggle triad, CD4 + T-cells could also differentiate into regulatory T cells (Treg) that are immunosuppressive in nature, with FOXP3 acting as the master regulator[5]. FOXP3 can inhibit and is inhibited by T-bet, GATA3 and RORγT directly or indirectly[9–14]. Also, double-positive cells co-expressing T-bet and FOXP3, GATA3 and FOXP3, and RORγT, and GATA3 have been reported, suggesting the presence of hybrid Th1/Treg, Th2/Treg and Th17/Treg states[5]. However, it remains unclear whether a four-node mutually repressive network among T-bet, GATA3, RORγT and FOXP3 is sufficient to explain the co-existence of these 10 states – four single-positive ones (Th1, Th2, Th17 and Treg) and six double-positive ones (Th1/Th2, Th1/Th17, Th2/Th17, Th1/Treg, Th2/Treg and Th17/Treg) and switching among them.

Here, we investigated the emergent dynamics of a toggle tetrahedron – four nodes (A, B, C and D) repressing each other, by simulating a set of coupled differential equations over a parameter ensemble. We show that this network predominantly allows six double-positive states: (high A, high B, low C, low D), (high A, low B, high C, low D), (high A, low B, low C, high D), (low A, high B, high C, low D), (low A, high B, low C, high D) and (low, low B, high C, high D). The presence of single-positive states, on the other hand, is much less prevalent. We further demonstrate switching among these states and identify the network design principles that enable their co-existence. Our results suggest that the differentiation of a progenitor cell into four distinct single-positive states is a two-step process: first, it acquires one of the six double-positive (hybrid) states, following which one of the two lineages is chosen. They also offer a mechanistic explanation for how a 'toggle tetrahedron' among T-bet, GATA3, RORγT, and FOXP3 allows for the stable existence of multiple intermediate T-cell subsets.

Results

Toggle tetrahedron enables six predominant 'double-positive' states

Previous reports have identified pairwise mutual inhibition between lineage-specifying transcription factors of Th1, Th2, Th17 and Treg: T-bet, GATA3, RORγT,and FOXP3, respectively[6,9–14]. We had earlier investigated the emergent dynamics of a toggle triad, reflecting interlinked toggle switches among T-bet, GATA3 and RORγT. Here, we incorporate the toggle switch that FOXP3 forms with each of these three factors, thus forming a toggle tetrahedron (TTr) – a four-node mutually repressive network (Fig. 1A).

While the mutual inhibitions of FOXP3 with the other three master regulators have been reported directly or indirectly, the antagonism of FOXP3 with T-bet, GATA3, and RORγT was usually studied one at a time, not with all three master regulators simultaneously. Thus, we analysed an RNA-sequencing dataset where all four phenotypes were present, such that the antagonism of FOPX3 with T-bet, GATA3, and RORγT could be investigated together. This RNA-sequencing data for distinct CD4 + T-cell subsets sorted from peripheral blood of healthy donors (GSE135390) including Th1, Th2, Th17, Treg, and hybrid Th1/Th17 ones[15]. We quantified the enrichment of previously identified Th1, Th2, Th17, and Treg-specific gene lists[16,17] in these subsets. We observed that the Th1 gene signature was relatively enriched in Th1 and hybrid Th1/Th17 subsets compared to Th2, Th17, and Treg (Fig. 1B, i). Similarly, the Th2 gene signature was enriched in Th2 cells, the Treg signature in Treg cells, and the Th17 signature in Th17 and hybrid Th1/Th17 cells (Fig. 1B, ii-iv). These trends suggest the enrichment of Th1, Th2, Th17 and Treg signatures in corresponding cell types.

Further, we project these scores on a scatterplot that highlights that Treg-specific gene signature enrichment is negatively correlated individually with the enrichment of Th1 ($R = -0.75$, $p < 0.0001$), Th2 ($R = -0.67$, $p < 0.001$) and Th17 ($R = -0.54$, $p < 0.05$) specific gene signatures (Fig. 1C, ii-iv) as well as with a common Th specific gene signature seen in Th1, Th2 and Th17 cells ($R = -0.97$, $p < 0.0001$) (Fig. 1C, i). Together, these results establish the mutual antagonism that the lineage-specific transcription factor for Treg (FOXP3) has with those of Th1, Th2 and Th17—T-bet, GATA3 and RORγT, respectively. Integrating these trends with a toggle

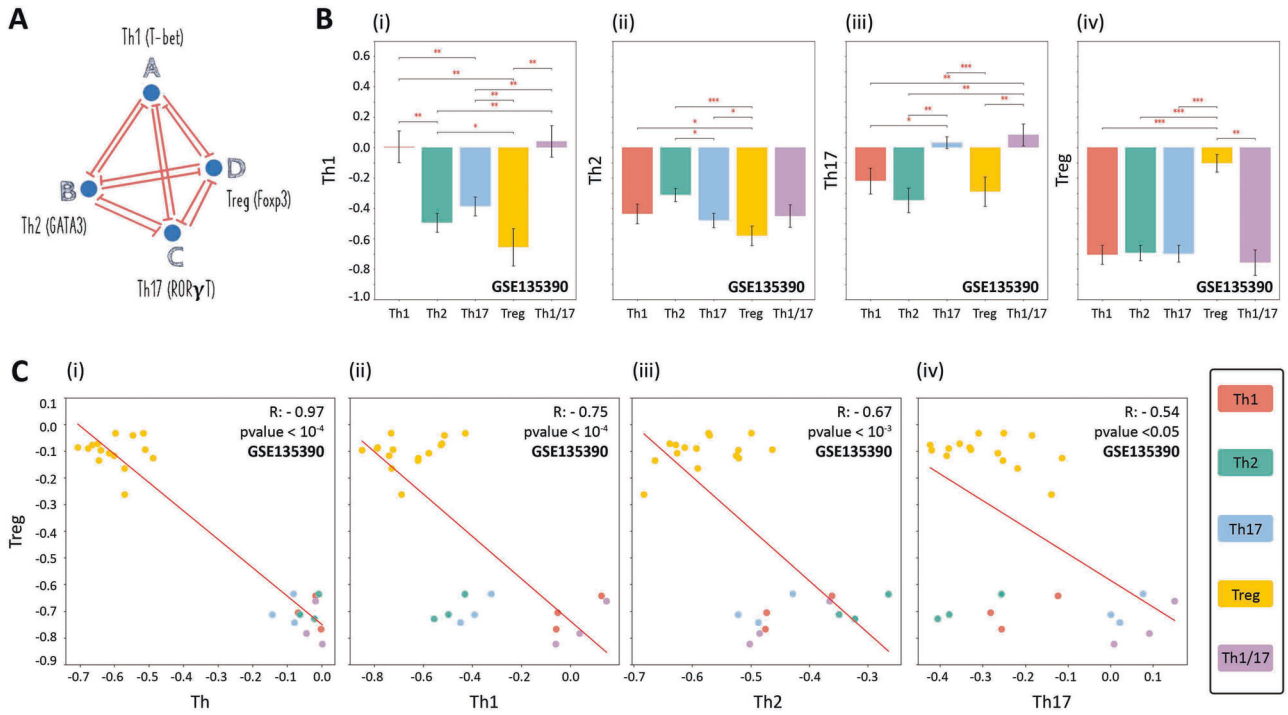

Fig. 1 | Transcriptomic analysis showing enrichment of Th1, Th2, Th17 and Treg signatures corresponding to specific cell type. A Schematic showing the regulatory network among the regulators of Th1 (T-bet), Th2 (GATA3), Th17 (RORγt), and Treg (Foxp3), forming a toggle tetrahedron. **B** Quantification of difference in levels of i) Th1, ii) Th2, iii) Th17 and iv) Treg gene signature enrichment scores across Th1, Th2, Th17, Treg and hybrid Th1/17 cells (GSE135390). **C** i) Scatterplot showing different cell types on the Th-Treg gene signature enrichment score plane. ii-iv) Same as i) but for Th1-Treg plane, Th2-Treg place and Th17-Treg plane (GSE135390). Pearson's correlation coefficient values are shown. *: p value < 0.05, **: p value < 0.01; ***: p value < 0.001 for Student's two-tailed t-test.

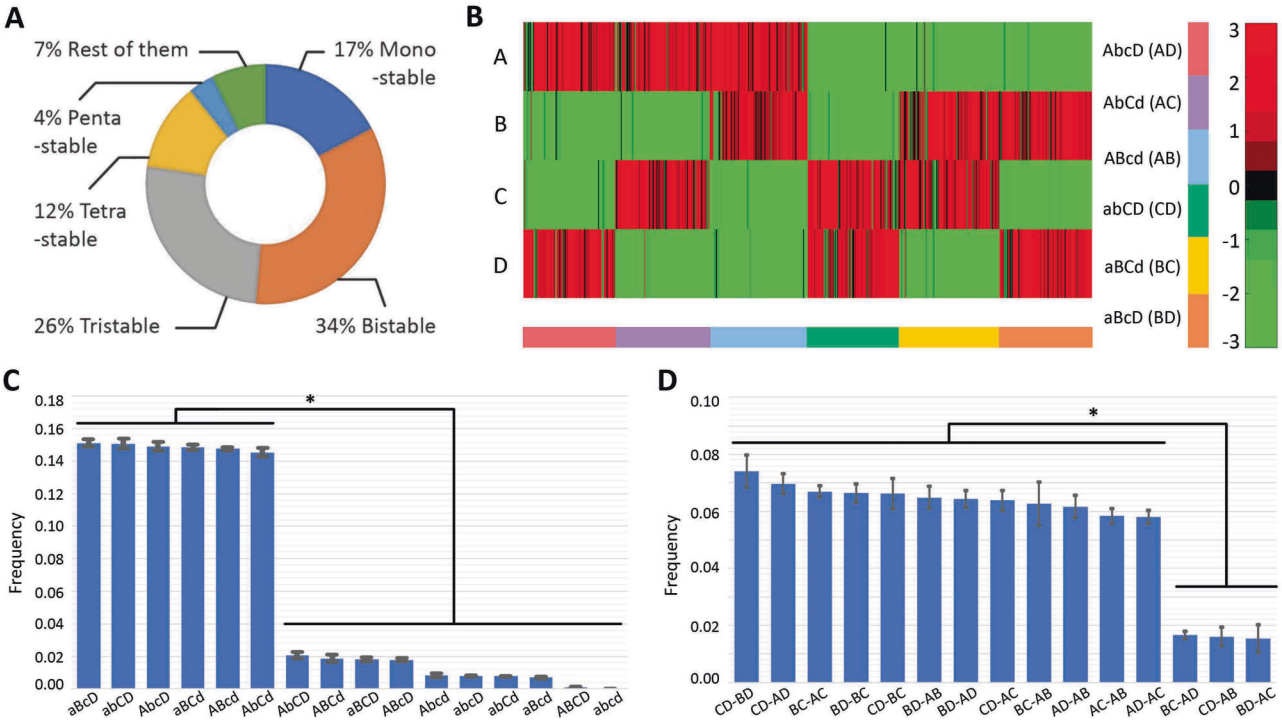

Fig. 2 | Characterization of phenotypes enabled by a toggle tetrahedron. **A** *Frequency of monostable, bistable, tristable, tetrastable, pentastable solutions, and more than 5 co-existing states in the toggle tetrahedron, shown as a pie chart.* **B** *Heatmap showing the solutions obtained via RACIPE and nomenclature shows nodes with high (low) expression levels in an uppercase (lowercase) fashion.* **C** *Frequency distribution of states (all solutions taken together) with the most frequent ones highlighted being – {aBcD}, {abCD}, {AbcD}, {aBCd}, {ABcd} and {AbCd}.* **D** Frequency distribution of 15 possible bistable combinations. For the panels C & D, RACIPE data was collected from three independent runs. * shows $p < 0.05$ for Student's two-tailed t-test.

triad observed among T-bet, GATA3 and RORγT[7], we establish the formation of a toggle tetrahedron among these four factors.

We next investigated the dynamical properties of a toggle tetrahedron (between A, B, C and D) using a computational tool, Randomized Circuit Perturbation (RACIPE) analysis[18]. The input to RACIPE is a network topology – a list of activating and inhibiting interactions among the different nodes. RACIPE converts the topology into a set of coupled ODEs (ordinary differential equations) that reflect the set of interactions in that network topology. It then samples 10,000 unique sets of kinetic parameters over a biologically relevant range of values and generates an ensemble of mathematical models, each with a unique combination of parameter set values. For each such set, RACIPE randomly samples multiple initial conditions for each node in the network, simulates the dynamics of the network topology and reports different possible steady-state values for each node. It should be noted that for some parameter sets, depending on initial conditions, the system may converge to more than one steady state, showcasing multistability for those specific sets. Thus, each kinetic model simulated via RACIPE represents a distinct parameter combination, denoting the inherent cell-to-cell variability in biochemical reaction rates. An ensemble of such models can, therefore, represent the behaviour of a cell population.

Here, each kinetic model is a set of four coupled ODEs. Each ODE tracks the levels of a node engaged in a toggle tetrahedron: A, B, C and D. Next, we characterized the different steady states/ phenotypes enabled by toggle tetrahedron over all parameter sets as identified by RACIPE. Among the 10,000 parameter sets generated for the toggle tetrahedron, the network enabled about 17% monostable cases, 34% bistable cases, 26% tristable cases, 12% tetrastable cases, 4% penta-stable cases and 7% cases of more than 5 co-existing states (Fig. 2A), thus highlighting the underlying multistable behaviour for this network topology. Given the high degree of non-linearity in the coupled ODEs for a toggle tetrahedron—each Hill co-efficient can take a value between 6 to 10, and when Hill functions are multiplied in the equation for the 4 nodes—we could get polynomials of a high degree which could lead to such multistable scenarios. To identify which specific states are enabled by the network overall multistable sets, we normalized the expression levels of the four nodes A, B, C and D for all solutions corresponding to up to 5 co-existing states (93% of solutions) and plotted them as a heatmap (Fig. 2B). The heatmap shows the predominance of six states where two nodes were expressed higher relative to the other two ('double-positive' states)—{high A, high B, low C, low D}, {low A, low B, high C, high D}, {high A, low B, low C, high D}, {low A, high B, high C, low D}, {high A, low B, high C, low D} and {low A, high B, low C, high D}—represented as {ABcd}, {abCD}, {AbcD}, {aBCd}, {AbCd} and {aBcD} respectively, hereafter. The dominance of 'double-positive' states was maintained upon varying the number of parameter sets chosen (10^5, instead of 10^4) and initial conditions per parameter set (10^4, instead of 10^3) (Supplementary Fig. 1).

Because each node in a TTr is capable of exhibiting 'high' or 'low' levels, the network can have a total of 16 ($=2^4$) states. We quantified the frequencies of these 16 states over all the parameter sets and observed a clear dominance of the six possible 'double-positive' states followed by the existence of 'triple-positive' and 'single-positive' states (Fig. 2C). The six 'double-positive' states ({ABcd}, {abCD}, {AbcD}, {aBCd}, {AbCd} and {aBcD}) each accounted for about 15% of all the states occurring. The four 'triple-positive' states ({ABCd}, {AbCD}, {ABcD} and {aBCD}) each accounted for about 2% of all states occurring. The 'all-high' and 'all-low' states ({ABCD} and {abcd}) and the four 'single-positive' states ({Abcd}, {aBcd}, {abCd} and {abcD}) were the least prevalent. Among the parameter sets enabling monostability, a similar trend repeats with each of the six 'double-positive' states accounting for 14–16% of the cases, while each of the four 'single-positive' and four 'triple-positive' states each account for about 1.5% of the cases (Supplementary Data 1), reflecting the symmetry of a toggle tetrahedron. We have considered only the 'double-positive' states for further analysis since the rest together do not have more than 10% frequency.

Next, we characterized the combinations of steady states given by bistable parameter sets. A bistable parameter set would give rise to two stable

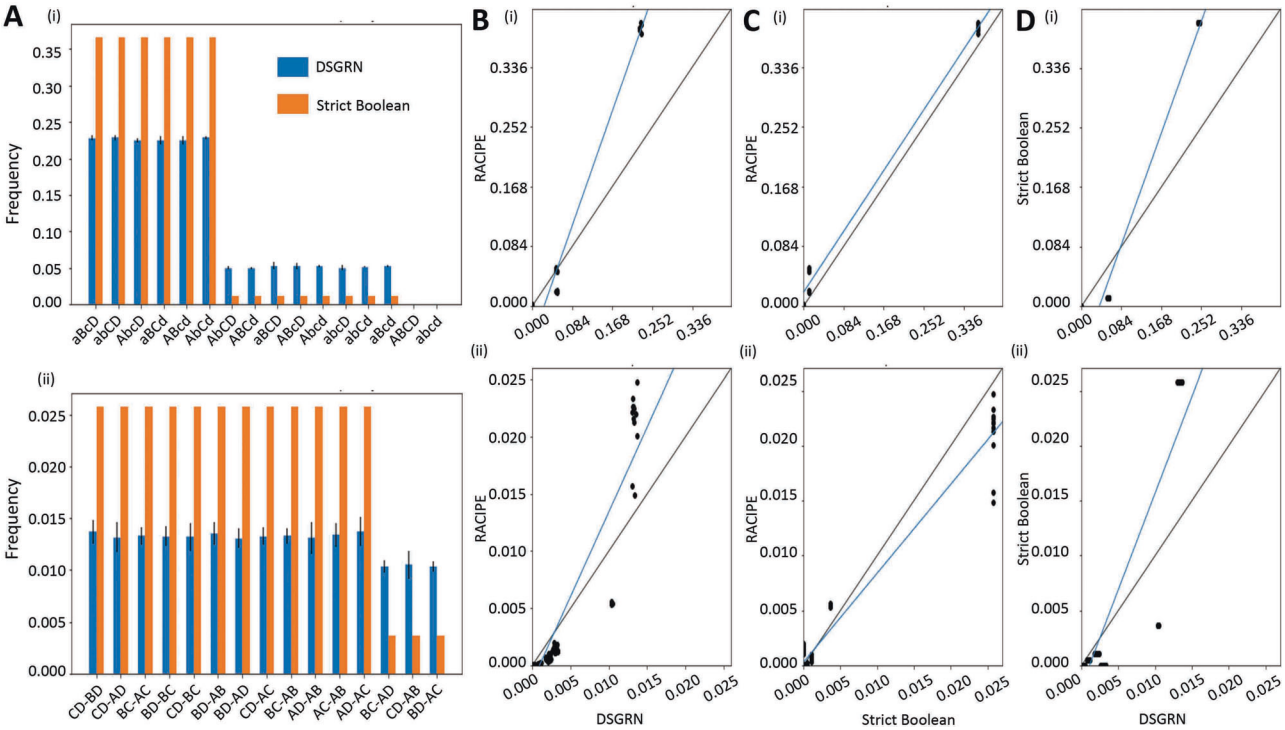

Fig. 3 | State-space analysis of toggle tetrahedron using DSGRN. A Frequency of all states (i, top) and frequency of bistable states (ii, bottom) for the DSGRN randomly sampled parameters (blue) and all 6561 strict monotone Boolean parameters (orange). Note that four sets of 10,000 parameters were sampled, the black line on the blue bars indicate the standard deviation in frequency between these sets. **B** Simple linear regression[61] was used to show the relationship between RACIPE and sampled DSGRN frequencies (black dots) for all states (i, top) and bistability (ii, bottom). The line of best fit is indicated by the blue line, while the black line represents the line y = x. **C** Same as (**B**) for RACIPE and strict Boolean frequencies. **D** Same as (**B**) with strict Boolean and sampled DSGRN frequencies. Notice that when the blue line slope and intercept are close to the black line, as we see in **C**, indicates that the frequencies between the pairs are very similar.

steady states. Thus, a total of 120 (= $^{16}C_2$) possible bistable combinations are possible, but only 15 combinations had a frequency of more than 1% as a fraction of all bistable combinations, and the remaining 105 (= 120 – 15) combinations only accounted for 19% frequency (Supplementary Data 1). Thus, we ignored these 105 combinations for further analysis and focused on those 15 ones also. Not surprisingly, these 15 (= $^{6}C_2$) combinations are sets of any two 'double-positive' states, given their predominance in monostable parameter sets as well as all parameter sets together. Intriguingly, out of the 15 possible combinations of bistable states - 3 states, which are a combination of 'mirror states' (i.e., when the bistable state is—{ABcd, abCD} / {AbCd, aBcD} / {AbcD, aBCd}, i.e. a combination of states where all four nodes switch their levels between the two states) were found to have significantly lower frequency - together accounting for about 4.5% of the parameter sets—each accounting for about 1.5%. The other 12 states consisted of a combination of nonmirror states, i.e., a combination of states where two nodes do not switch their levels (say {aBcD, AbcD}, where A and B switch their levels between the two states, but C and D do not) and together accounted for 84% of the parameter sets—each accounting for about 7% (Fig. 2D). Put together, our results suggest that the toggle tetrahedron network topology allows for the co-existence of 'double-positive' states/ phenotypes where the expression level of two of the regulators is higher relative to the other two.

In addition, we use the complementary tool Dynamic Signatures Generated by Regulatory Networks (DSGRN)[19,20] to analyse the behaviour of TTr across the set of all parameters, as we did earlier for a toggle switch and toggle triad[21]. DSGRN analyses the behaviour of ODE models with piecewise constant nonlinearities, which result from taking a limit of the Hill function nonlinearities used by RACIPE as the Hill coefficient tends to infinity. This approximation enables DSGRN to divide high-dimensional parameter space into a finite number of regions defined by explicit inequalities among parameters and identify the corresponding stable steady states/phenotypes associated with all real-valued parameters within that region. By ignoring the value of the Hill coefficient, RACIPE parameters may be directly assigned to a DSGRN parameter region, permitting an analytical comparison of phenotype predictions of the TTr model to RACIPE output. Since DSGRN computes steady states by combinatorial methods and does not use ODE simulations, the computational time using DSGRN is several orders of magnitude smaller compared to that of RACIPE. However, the TTr provides a challenge to the combinatorial methodology of DSGRN, as the number of parameter regions of the TTr is over 27 trillion. Instead of an exhaustive computation of steady states for all these regions, we introduce two approaches. First, we explore a very small (6561 regions out of 27 trillion) but well-studied subset of the parameter regions that we term Strict monotone Boolean (SB) parameters. This approach corresponds to a choice of monotone Boolean functions at each vertex of TTr and we study the number of steady states for the corresponding Boolean dynamics. Second, we perform stochastic sampling of DSGRN parameter regions. Finally, we compare the frequencies of different types of steady states predicted by DSGRN SB parameters and by DSGRN stochastic parameter sampling to RACIPE stochastic samples.

We first compared the predictions of the DSGRN SB parameter subset to the predictions obtained by a stochastic sampling of DSGRN parameter space. We notice substantial differences in predictions. DSGRN SB parameters indicate a much greater frequency of double-positive states than stochastic sampling (Fig. 3A, i). Additionally, DSGRN SB parameters predict that 12 of the 15 possible bistable states (the ones that are not a combination of 'mirror states') exhibit much higher frequencies than the remaining 3 bistable states, while DSGRN stochastic sampling only shows a small difference between these two subsets of bistable states (Fig. 3A, ii). Next, we compared the all-state frequency predictions of DSGRN to those of

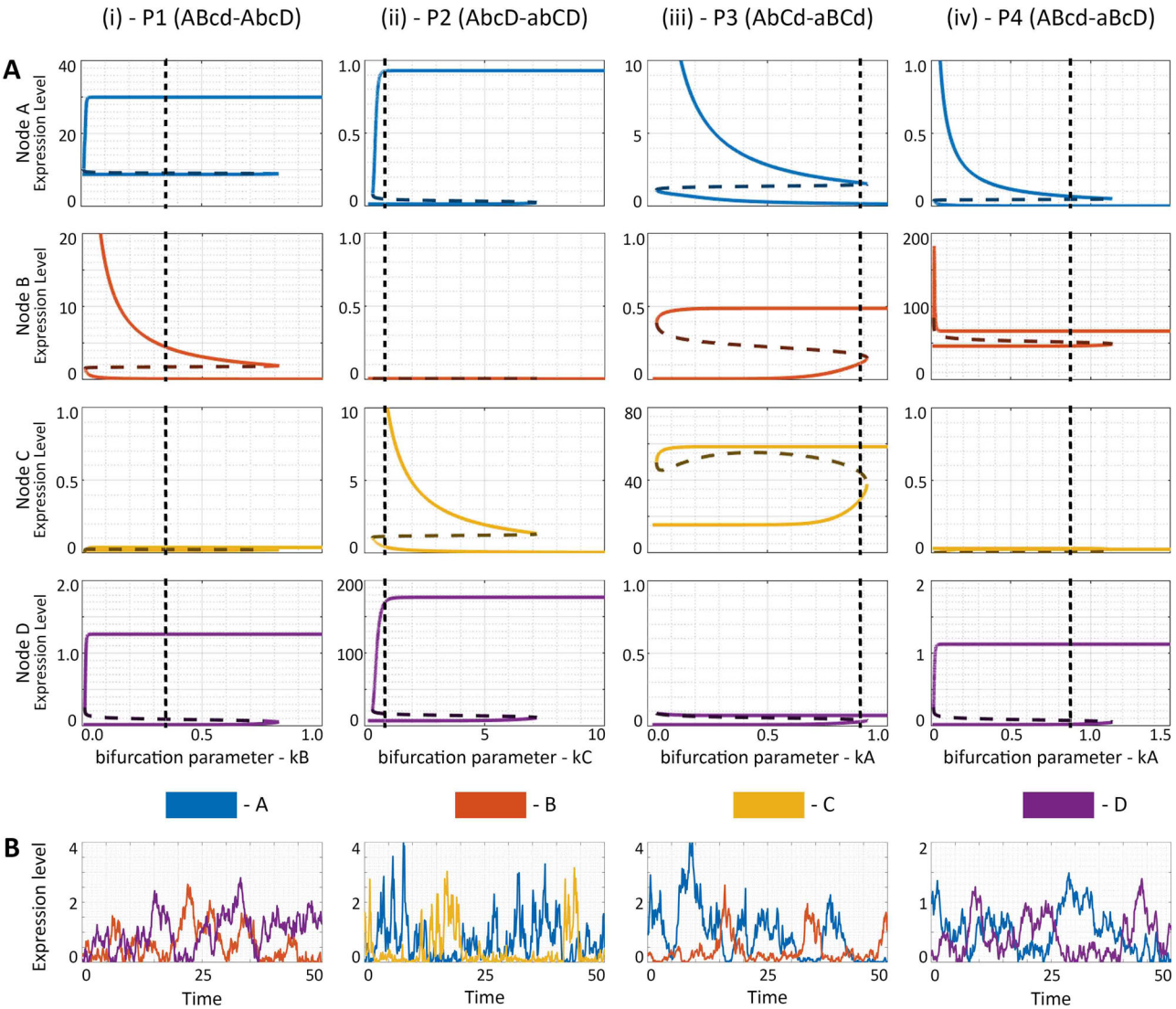

Fig. 4 | Bifurcation analysis of representative parameter sets corresponding to the non-mirror bistable states. A Bifurcation diagrams of four representative cases (each column denotes a different parameter set – P1-P4) with each row showing the expression levels of the four nodes A–D. Dotted vertical line in each case marks the RACIPE parameter value of the corresponding bifurcation parameter. **B** Stochastic simulations showing switching between the bistable states (only the two nodes switching between 'high' and 'low' are shown, the nodes always expressed 'high' or always 'low' are not shown). Parameter sets P1, P2, P3 and P4 are provided in Supplementary Data 2.

RACIPE (top row) and, similarly, the frequency predictions of bistable states (bottom row). This comparison was done to both DSGRN stochastic sampling (Fig. 3B) and to DSGRN SB parameters (Fig. 3C). We observe that low frequency predictions in RACIPE are correlated with low frequency predictions in the DSGRN methods, and similarly for higher frequency predictions. However, the best affine fit between DSGRN and RACIPE predictions has a linear coefficient other than 1 (blue regression lines vs black line in Fig. 3B, C). The DSGRN SB parameter predictions have a linear coefficient closer to 1 than the stochastic samples and, in this sense, may indicate a closer relationship between the predictions of RACIPE and DSGRN SB than between RACIPE and DSGRN stochastic sampling. Lastly, and for completeness, we show the best affine fit between DSGRN stochastic sampling and DSGRN SB parameters for all states (Fig. 3D, i) and bistable states (Fig. 3D, ii). As expected from the comparisons to RACIPE, the low and high frequencies are well correlated, but the linear coefficient differs from 1.

We show that the steady states of SB parameters where each monotone Boolean function is non-degenerate, i.e. non-constant and where each input is able to affect the output, can be analytically determined (**SI Section 3**). We use this analysis to confirm the numerical results (Figs. 2C and 3A) that the double-positive equilibria occur more frequently than other types of equilibria. We further analyse other symmetric tetrahedron networks where the number of positive in-edges at each node is either 1, 2 or 3. Our analysis shows that in each of these cases within the ensemble of all compatible non-degenerate monotone Boolean functions, the frequency of double-positive states is higher than the frequency of other states (**SI Section 3**).

Dynamical traits of double-positive states enabled by toggle tetrahedron

To further characterize the parametric space corresponding to the co-existence of the double-positive states, we performed a bifurcation analysis of multiple parameter sets enabling non-mirror bistable states identified by RACIPE. For a representative parameter set enabling the bistable state – {ABcd-AbcD}, where the expression level of nodes B and D should switch, we chose the degradation rate of B (kB) as the bifurcation parameter (Fig. 4A, i). This choice was motivated by experimental tools available to vary the stability (or half-life) of a protein through post-translational modifications.

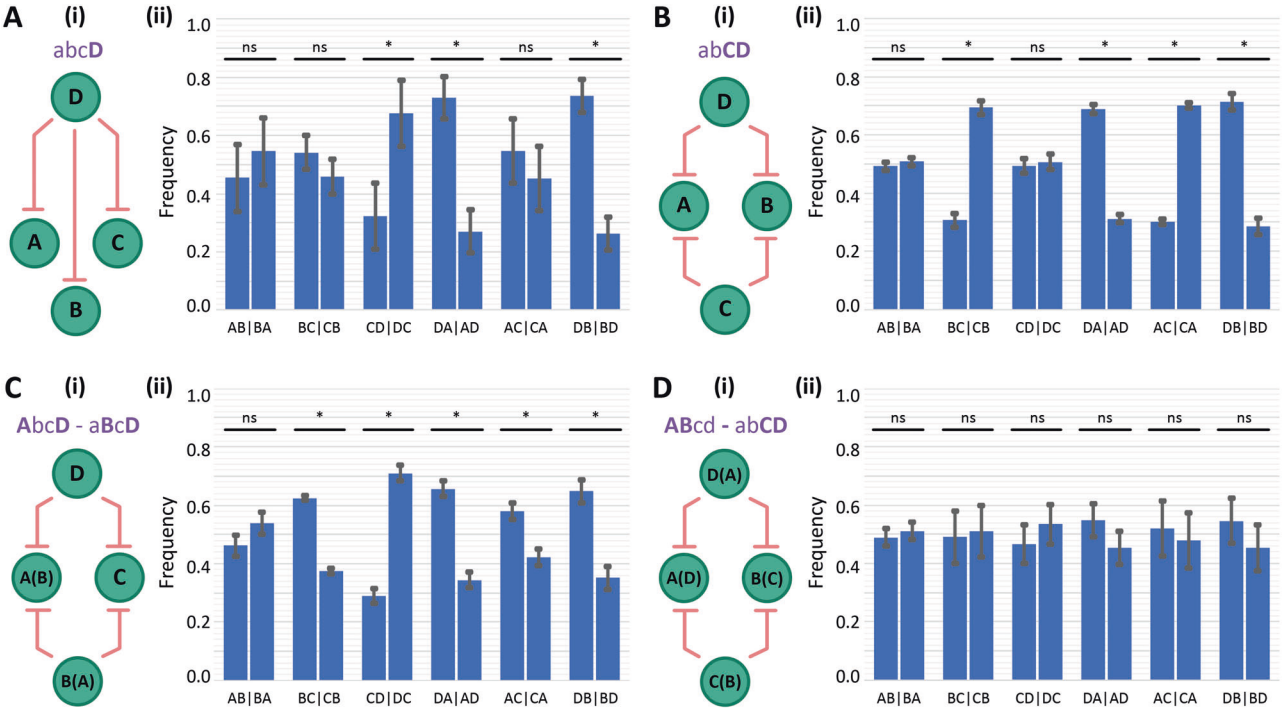

Fig. 5 | Link Strength Analysis of monostable and bistable states for toggle tetrahedron. A i) Schematic showing the links that are expected to be stronger than their counterparts for the state {abcD} ii) Frequency of dominance of all six pairs of mutually inhibitory links between any two nodes in a toggle tetrahedron, for all parameter sets corresponding to the case of monostable {abcD}. **B** Same as A) but for the monostable state – {abCD}. **C** Same as A) but for the non-mirror bistable state combination – {AbcD, aBcD}. **D** Same as A) but for the mirror bistable state combination – {ABcd, abCD}. In **C** and **D** panels, the nodes that switch between the two states are written as X(Y), where X and Y can switch.

We observed that at high levels of kB, the system loses bistability and becomes monostable as the state {ABcd} no longer exists. Conversely, at very low levels of kB, only the state {ABcd} exists, and the system loses bistability. In the bistable regime (kB ranging between 0.1 and 0.8, thus spanning almost an order of magnitude), the expression levels of B and D switch between two states – one is relatively high and the other low. The nodes A and C also exhibit two states, but the levels of A are high in both the states, and those of C are relatively too low to distinguish between them. For the kB value obtained from the RACIPE generated parameter set, we performed stochastic simulations to validate the switching between states and observed the expression levels of B and D (Fig. 4B, i). We see that the levels of B and D are mutually exclusive, i.e., when B is relatively high, D is low and vice versa, as expected from the bistable state where B and D switch between states.

We performed the same analysis for three more representative parameter sets enabling the bistable states – {AbcD, abCD}, {AbCd, aBCd} and {ABcd, aBcD}, and observed similar behaviours though the bifurcating parameters were degradation rates of different nodes (kC, kA and kA respectively) (Fig. 4A, ii-iv). In each of the cases, we see that the expression level of the node which is always 'high', switches between two levels, but both these levels are relatively 'high'. Stochastic simulations showed possible switching between the two bistable states enabled by the respective parameter set (Fig. 4B, ii-iv). Put together, these results highlight that the co-existence of 'double-positive' states is a robust feature of TTr, and this feature can be disrupted by altering the degradation rate of nodes in the TTr network (i.e. the half-life of one of the TFs engaged in a TTr is drastically manipulated).

Design principles of multistability enabled by toggle tetrahedron

A toggle tetrahedron can exhibit monostable (17% of parameter sets) or multistable (83% of parameter sets) dynamics. Thus, we investigated various parameter sets from the RACIPE analysis to deduce a relationship between the parameter sets and the different states they converged to. We hypothesized that the relative strength of transcriptional inhibition among the different nodes controls the different stable steady states observed. To quantify the strength of inhibition from one regulator onto the other, we used a metric called link strength X, where X(AB) represents the value of inhibition from regulator A to B, in accordance with the formulation of RACIPE framework[7].

In RACIPE formalism, the strength of the inhibitory interaction is defined by a shifted Hill function consisting of three parameters – n (Hill coefficient corresponding to cooperativity), λ (fold-change) and T (half-maximal concentration or threshold). For an inhibitory link, the higher the value of n, the faster is the increase in strength of inhibition with changing concentration of the source node, or in other words, the steeper the increase in strength of inhibition. For inhibitory links, λ value ranges from 0.01 (strong repression) to 1 (no effect). Thus, the smaller the value of λ, the stronger the inhibition. Similarly, the smaller the value of T, the lower is the concentration of the source regulator needed for the inhibition to be active. Thus, we defined the link strength metric, X = n/(λ *T), such that the higher the value of X, the stronger is the strength of inhibition.

For the parameter sets that enable the monostable 'single-positive' state {abcD} or {low A, low B, low C, high D}, we hypothesize that the inhibitions of A, B and C by D are relatively stronger than inhibition of D by A, B and C. To test the hypothesis, we first shortlisted the parameter sets that enable the particular state (here, monostable {abcD}) and then calculated the strength of inhibition between each pair of nodes for each parameter set. For every parameter set, and for each pair of nodes, among the two inhibitory links, we identified the dominant one and thus quantified the frequency with which one node inhibits the other one more strongly compared to vice versa. We found that for approximately 70% of the parameter sets, the conditions X(DA) > X(AD), X(DB) > X(BD) and X(DC) > X(CD) were true, i.e. inhibitions originating from the node D were stronger than their opposing counterpart in a mutually inhibitory feedback loop (Fig. 5A). On the other hand, no such skew was observed for mutual inhibition among pairs of

nodes whose levels were low, i.e. between A and B, between B and C and between A and C, i.e. in approximately 50% of parameter sets, X (AB) > X (BA), and in the remaining 50%, X (BA) > X (AB) (Fig. 5A). Results for other monostable 'single-positive' states show similar trends (Supplementary Fig. 2A–C). For the case of monostable 'double-positive' state {abCD} or {low A, low B, high C, high D}, we hypothesized that the inhibition of A and B by C and D is stronger than that of C and D by A and B. We found our hypothesis to be true in 70% of the parameter sets corresponding to this state, i.e. the conditions X(CA) > X(AC), X(DB) > X(BD), X(CB) > X (BC) and X (DA) > X (AD). However, the two remaining pairwise mutual inhibitions – one between A and B, and the other between C and D – did not show any such skew (Fig. 5B). Consistent trends were observed for other monostable 'double-positive' states (Supplementary Figs. 2D–F, 3B–F). Similarly, for a monostable 'triple positive' state {aBCD} or {low A, high B, high C, high D}, we noticed that in about 70% of corresponding parameter sets, the inhibition of A by B, C and D was higher than inhibition of B, C and D by A, i.e. X (BA) > X (AB), X (CA) > X (AC) and X (DA) > X (AD). However, no such skew was noted for pairwise mutual inhibition among B, C and D (Supplementary Fig. 3A). These trends highlight the parametric conditions under which TTr topology does not allow for multistable behaviour and instead converges to one of the different possible monostable scenarios. Theoretical analysis of nondegenerate monotone Boolean functions also confirms the RACIPE results that for any pair of genes, the strength of repressive connection from highly expressed gene is larger than that from a weakly expressed gene (**SI section 4**). However, it should be noted that these conditions identified for this phenomenological model may not be sufficient to enable these monostable scenarios when looking at a more complete regulatory network that is closer to reality in terms of size and complexity.

Next, we performed the link strength analysis for parameter sets enabling bistability. In the case of bistable states, we have two predominant combinations among the 'double-positive' states – a pair of mirror states and a pair of non-mirror states.

For parameter sets enabling the non-mirror state combination of {aBcD, AbcD}, we hypothesized the following: a) inhibition of A, B and C by D is overall stronger than inhibition of D by A, B and C; ii) inhibition of C by A, B and D is overall stronger than that inhibition of A, B and D by C; iii) for mutual inhibition between A and B, both the links are equally likely to be stronger than the other. An analysis of corresponding parameter sets reveals our hypothesis to be true: i) X(DC) > X(CD) in approximately 70% of parameter sets, X(DA) > X(AD) and X(DB) > X(BD) in approximately 65% of the parameter sets, ii) X(AC) > X(CA) and X(BC) > X(CB) in approximately 60% of parameter sets, and X(DC) > X(CD) in about 70% of parameter sets, and iii) X(AB) > X(BA) in about 50% of the parameter sets (Fig. 5C). In the case of parameter sets enabling bistability with the pair of mirror states – {abCD, ABcd}, we hypothesized that for mutual inhibition between every pair of nodes, each inhibition is equally likely to be stronger than the other. The results showed that for the two inhibitions between any pair of nodes, one is stronger than the other in about 50% of the parameter sets (Fig. 5D). Similar trends were observed for the other bistable state combinations (Supplementary Figs. 4–6). Put together, these results point towards patterns in a high-dimensional parametric space that allows a toggle tetrahedron to enable specific combinations of states or dynamical behaviours.

Uniqueness of the dynamical traits of toggle tetrahedron

T-bet, GATA3, RORγT and FOXP3—similar to many master regulators—are known to self-activate directly and/or indirectly[7,22,23]. Thus, we investigated the dynamics of TTr when all 4 nodes can either self-activate (TTr +SA) or self-inhibit (TTr+SI). We observed that compared to TTr, for TTr +SA, the number of parameter sets corresponding to monostability, bistability and tristability decreased, but those corresponding to higher-order multistability (tetrastability and pentastability) were enhanced. However, for the TTr+SI network, the number of parameter sets enabling multistability decreased, and those corresponding to monostability increased (Supplementary Fig. 7D, E). The frequency of single-positive and triple-positive states changed in these two scenarios though. For TTr+SI (TTr +SA), the frequency of triple-positive states increased (decreased), and the frequency of single-positive states decreased (increased) (Fig. 6A, Supplementary Fig. 8). Irrespective of these changes, the 'double-positive' states were still the most predominant ones in case of both TTr+SA and TTr+SI (Fig. 6A), showcasing that the salient features of a TTr remain unchanged upon adding self-regulations

We next asked how unique the predominance of 'double-positive' states is to a TTr topology. To answer this question, we calculated the steady-state distributions of all possible fully connected four-node networks, i.e. networks in which each node is connected to at least one of the other 3 nodes. No self-regulatory edge was allowed in this ensemble of networks; given that each of the 12 edges connecting any two nodes can be activatory or inhibitory, we have a large possibility space of network topologies. We shortlisted them, using the NetworkX library in Python[24], to ensure that each network is unique, i.e. no network is repeated in the network topology space. We found a total of 218 possible networks, including the TTr. Next, we compared the behaviour of the 217 networks, one at a time, with the TTr as the reference by measuring how different or similar the frequency distribution of the 16 possible states. To minimize the computational costs of simulating 217 networks, these simulations were done using discrete Boolean modelling with a general asynchronous update scheme and simple majority update rule, instead of RACIPE. Previous simulations for other network topologies showed remarkable consistency in steady-state distributions obtained via RACIPE and Boolean modelling[25–27], thus we chose this modelling strategy. We used JSD (Jensen-Shannon Divergence) as our metric to compare corresponding steady-state distributions. JSD values lie between 0 and 1; the higher the value, the more different the two distributions are. We noticed that as we transition from TTr to other four node networks in which one or more of the inhibitions between two nodes is swapped with activatory edge(s), the higher the number of such swaps, the higher the JSD (Fig. 6B). Intriguingly, for as less as three swaps, we begin to see networks with JSD = 1, i.e. completely non-overlapping steady-state distributions, when compared with the TTr. JSD was found to be 0 only when there were no swaps. Put together, this result shows that the features observed for TTr are unique to its network topology and increasingly differ with an increasing number of swaps of inhibitions by activations in the network topology.

Regulatory networks such as a TTr do not operate in isolation but are often embedded in larger networks. Thus, we quantified the behaviour of TTr when embedded in external networks of varying sizes and densities (Fig. 6C, i). We chose these external networks of 3 sizes (10 nodes, 15 nodes, 20 nodes) and 3 densities (no. of edges = 2* no. of nodes, no. of edges = 4* no. of nodes, no. of edges = 6* no. of nodes). These representative values of size and density of the external network were chosen to discern the impact of these two parameters on the functional traits of the embedded motif. We noticed saturating behaviour beyond a specific size or density, based on our prior work of embedding a toggle switch or triad within a large network[28]. Here, for a given size and density, we chose 100 unique random networks in which we embedded the TTr. Thus, in total, we simulated 900 (= 3*3*100) networks and used the abovementioned Boolean modelling strategy to minimize computational costs. For each of these 900 networks, we measured the net frequency of the six 'double-positive' phenotypes, and plotted the distribution of these frequencies for the set of 100 external networks corresponding to a fixed size and density. We noticed that as the size and, more importantly, the density of the external network increased, the sum of frequencies of the 'double-positive' states decreased (Fig. 6C, ii). However, the extent of the decrease is not so high that the 'double-positive' states do not dominate the frequency distribution. In most cases, the six 'double-positive' states remain much more frequent than the four 'single-positive' ones (Fig. 6C, iii; Supplementary Fig. 9), reflecting the functional resilience of a TTr topology when embedded in external networks. This behaviour is reminiscent of the resilience of the toggle switch when embedded in similar external networks, where 'single-positive' states are the most dominant (Supplementary Fig. 7A) and of embedded toggle triad where 'single-

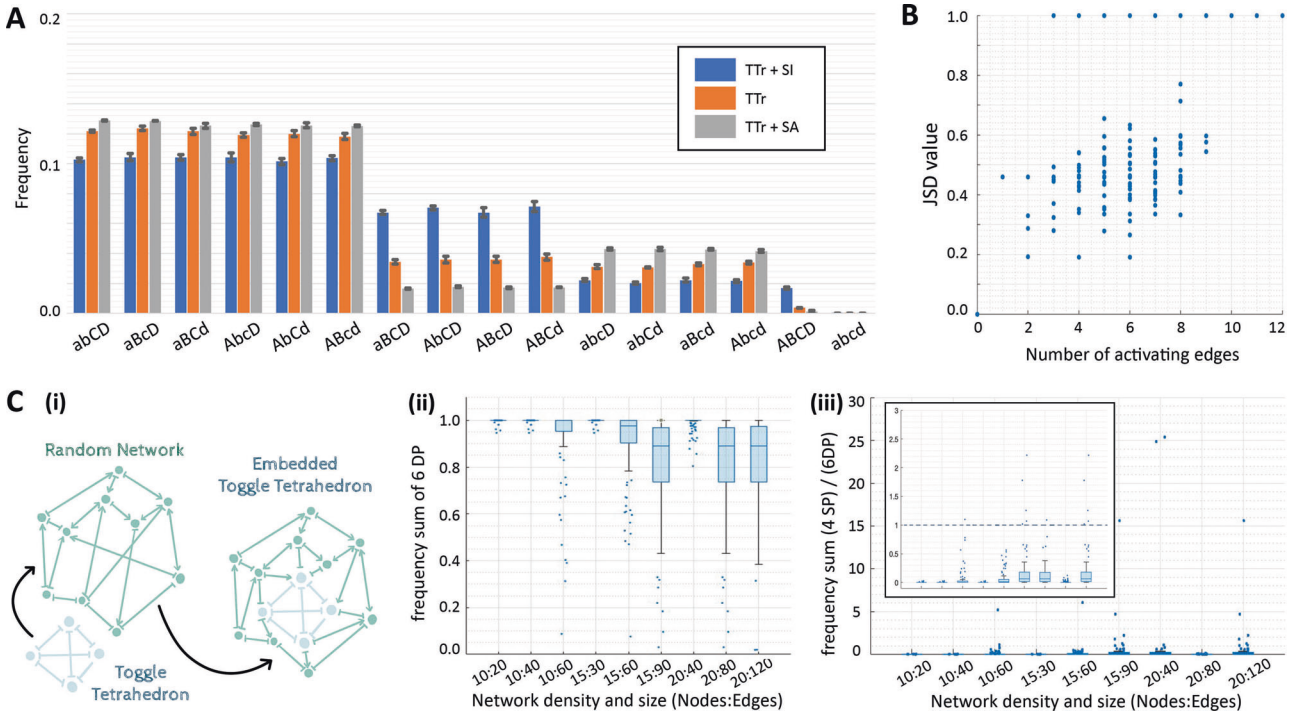

Fig. 6 | Features unique to the toggle tetrahedron topology. A Frequency of monostable, bistable, tristable and other multistable states for TTr, TTr + SI and TTr + SA. **B** Scatterplot showing the JSD value between the frequency distribution graphs of the reference network (TTr) and the network specified by the number of inhibiting edges swapped (on x-axis) when all steady states are taken together. **C** i) Schematic representing how a TTr network is embedded in a larger random network. ii) Sum of the frequencies of all the six 'double-positive' states for Boolean simulations of networks of varying sizes and densities. iii) Fraction of sum of frequencies of all the four 'single-positive' states (4 SP) over the sum of frequencies of all the six 'double-positive' states (6 DP) for Boolean simulations of networks of varying sizes and densities. Inset shows a zoomed in version with the y-axis range – (0,3).

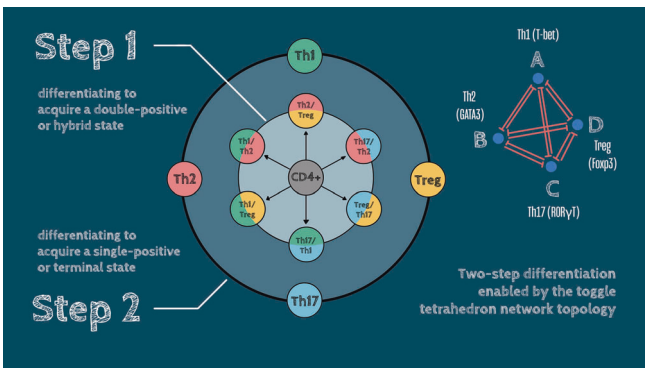

Fig. 7 | Schematic representing the two-step differentiation enabled by the toggle tetrahedron. (left) CD4 + T-cells can acquire hybrid or 'double-positive' states and differentiate into a single-positive state, as enabled by dynamics of toggle tetrahedron among T-bet, GATA3, RORγt, and Foxp3 (right).

positive' and 'double-positive' states retain their dominance (Supplementary Fig. 7B, C)[28].

Discussion

Multistability is a hallmark of diverse cell-fate decision regulatory networks[2], and synthetic multistable circuits are being increasingly integrated into *E. coli*, yeast and mammalian cells[29–32]. It is not only observed at an intracellular level, but also in spatial tissue-level patterning through the emergent dynamics of cell-cell communication networks such as Notch-Delta-Jagged signalling[33,34]. Thus, decoding the dynamical traits of multistable networks is critical to better understand cellular development and reprogramming and has attracted extensive theoretical attention too[35].

Most deterministic or stochastic computational models of multistable networks have assessed the dynamics of a mutually inhibitory loop between two transcription factors (TFs), or a TF and micro-RNA, where the TFs may self-activate[2,36–39]. Such toggle switches are extensively observed at cell-fate bifurcation points in developmental decision-making[3], where a common progenitor can give rise to two mutually exclusive phenotypes. Consistently, a toggle switch between nodes A and B can allow for the co-existence of (high A, low B), (low A, high B) and (medium A, medium B) states. Here, we have investigated the dynamics of four lineage-specific TFs mutually repressing one another, as observed in CD4 + T-cell differentiation[5], thus forming a toggle tetrahedron.

Our results suggest that a toggle tetrahedron allows for the predominant existence of six 'double-positive' states where two of the four lineage-specific TFs have relatively higher expression levels as compared to the other two. This behaviour is fundamentally different from a toggle switch or a toggle triad, where 'single-positive' (only one of the lineage-specific TF is at relatively high levels) states dominate. A possible reason for the predominance of 'double-positive' states is that they are less frustrated[40] as compared to 'single-positive' or 'triple-positive' ones. Extending these results to understand the differentiation of naïve CD4 + T cells into Th1, Th2, Th17 and Treg subsets, we can indicate that this differentiation is a two-step process, where a multipotent cell first acquires one of the hybrid or 'double-positive' state (step 1), and further differentiate into one of the 'single-positive' states after the hybrid/progenitor cell switches to one of the two possible phenotypes (step 2) (Fig. 7). In this case, the naïve CD4 + T cell is presumed to express comparable levels of all four nodes, similar to observations for a progenitor state in a toggle switch where A » B and B » A are stable states but A ~ B is often unstable[41]. To the best of our knowledge, there is no experimental proof for our model prediction of T-cell differentiation following a two-step process. However, many 'double-positive' cell-states have been experimentally shown to be stable phenotypes – hybrid

Th1/Th2[42], hybrid Th17/Treg[43] and hybrid Th1/Treg[14]. This information, though not sufficient, supports what our model suggests. Our model predictions are consistent with these experimental results and provide dynamical insights into how these hybrid states can be achieved. Further time-course high-throughput analysis of CD4 + T-cell differentiation[8,15,44] into multiple (> 2) subsets simultaneously would help in testing our prediction of two-step differentiation. It should be noted that our approximation of CD4 + T-cell differentiation into Th1, Th2, Th17 and Treg via a toggle tetrahedron misses certain features, such as other nodes and/or edges affecting the network behaviour[45,46] and epigenetic remodelling that could have a time-varying influence on network dynamics[47]. Future efforts could incorporate these features for a more quantitative and comprehensive recapitulation the of dynamics of T-cell differentiation.

Previous computational models of CD4 + T-cell differentiation have often focused on the dynamics under a specific parameter set and have reported the presence of hybrid phenotypes[12,48,49]. Our analysis builds on those efforts and quantifies the frequency of different states across a wide parameter set ensemble, thereby demonstrating the salient features of the TTr network topology. Importantly, this predominance of a 'double-positive' state in a TTr is not seen in any other four-node network, and is retained even when it is embedded in larger networks, thus demonstrating the resilience of TTr network dynamics. Future computational models of CD4 + T-cell differentiation should incorporate additional lineage-specific TFs such as BCL-6 and Blimp-1 (that regulate the T follicular helper cell differentiation) and their interactions with T-bet, GATA3 and FOXP3[50–54], as well as the impact of spatial inhomogeneities in cytokine signalling[55]. Increasing the size of the network presents challenges to the analytical and numerical exploration of their dynamics. Larger networks come with a larger number of parameters, and RACIPE sampling thus covers less of the parameter space. The number of parameter regions (i.e. DSGRN parameters) examined by DSGRN methodology also grows exponentially with the size of the network. However, we observed that within the small subset of 6561 SB parameters out of 27 trillion of all parameters for TTr, there is a surprisingly high correlation between the results from RACIPE sampling, SB parameters, and sampling of all DSGRN parameters. We are currently seeking an explanation of this phenomenon, since examining only SB parameters would allow analysis of larger networks.

Overall, our results offer novel insights into TTr dynamics and propose a step-wise decision-making for a common progenitor cell capable of giving rise to more than two differentiated phenotypes. Besides, these insights can help in the design of synthetic four-node regulatory networks exhibiting multistability, building on prior work on two- or three-node synthetic multistable networks[29,30].

Methods

Randomized circuit perturbation (RACIPE) analysis

RACIPE[18] is a computational tool used to investigate the dynamical behaviour exhibited by a specific network topology. It attempts to quantify all possible steady-state behaviours the network topology can show over an ensemble of parameter sets, instead of a specific parameter set. Thus, it samples parameters over a biologically relevant range to generate multiple parameter sets. A large number of parameter sets is likely to ensure that all diverse behaviours in parametric space are accounted for. Analysing these results provides an understanding of the different states enabled by the topology in specific parametric spaces and an idea of the frequencies with which these states occur.

The formulation of one-way interaction between any two nodes of the network topology (say an inhibition from node B onto node A) is given by the following equation:

$$\frac{dA}{dt} = g_A * H^S\left(B, B_A^0, n_{BA}, \lambda_{AB}\right) - k_A * A \tag{1}$$

where g_A and k_A are intrinsic production and degradation rates of node A, respectively, and the Hill function $H^S\left(B, B_A^0, n_{BA}, \lambda_{AB}\right)$ represents the interaction (here inhibition) of the node B onto node A. The first term on the RHS represents the net production rate of node A, while the second term represents the degradation of node A (here, a first-order degradation is considered). The Hill interaction consists of a combined form of negative and positive Hill functions and is referred to as a shifted Hill equation. The Hill function is used to represent the activation or inhibition between two nodes because of the use of biochemical rate equation formulation of gene expression.

$$H^S\left(B, B_A^0, n_{BA}, \lambda_{AB}\right) = H^-(B) + \lambda_{AB} * (1 - H^-(B)) \tag{2}$$

where

$$H^-(B) = \frac{1}{1 + \left(\frac{B}{B_A^0}\right)^{n_{BA}}} \tag{3}$$

In case of the interaction being an activation, the hill function is further divided by the fold-change parameter corresponding to the respective interaction, i.e., in case of an activation from node B to node A, the hill function would be, $H^S\left(B, B_A^0, n_{BA}, \lambda_{AB}\right)/\lambda_{AB}$.

The Hill coefficient is chosen to vary from 6 to 10 for TTr, instead of the default range from 1 to 6 in RACIPE. This is because it allows for a bimodal distribution for the node expression levels to segregate 'high' and 'low' states (Supplementary Fig. 1A). We used the default values of number of parameter sets (=10000) and number of initial conditions per parameter set (=1000) for our simulations, although similar behaviour was observed when taking a larger number of parameter sets and/or initial conditions (Supplementary Fig. 1B). The threshold values are calculated such that for each parameter set, every interaction has a 50% chance of being active/inactive. For every parameter set, classification of its monostability, bistability or other multistability is done after simulating it for the 1000 initial conditions and finding the number of stable steady-states obtained.

Finding SF value for TTr embedded in larger networks

We embedded the TTr motif in randomly generated networks of specific sizes and densities, i.e., a specific number of nodes and edges in the network. For a given pair of values for the number of nodes and edges, we generated 100 networks randomly without overlap and for each network, we ran Boolean simulations following an asynchronous update rule[56]. We then calculated the sum of frequencies for the six 'double-positive' states (SF) enabled by the TTr motif.

NetworkX—for finding unique four node topologies

The constraint for us to find all possible network topologies is that they have to have four nodes, and each node is connected to every other node via activation or inhibition. We first generated all possible topologies, with every edge having a possibility of an activation or inhibition. To simplify the code, we did not consider the notations of activations and inhibitions but just marked the presence of an edge as an activation and considered its absence as an inhibition. We then generated all possible combinations of edges between nodes. For every classification based on the number of edges present, we compared the network topologies within each class using the 'nx.algorithms.is_isomorphic' function from NetworkX[24]. The 'nx.algorithms.is_isomorphic' function utilizes an implementation of the VF2 + + algorithm[57] for Graph Isomorphism testing to shortlist the unique network topologies in our case. Finally, after obtaining the unique topologies, we converted them to complete directed topologies (i.e., marked activations and inhibitions again). We exported these directed network topologies in the '.topo' file format for further RACIPE analysis.

Dynamic signatures generated by regulatory networks (DSGRN) analysis

DSGRN is a computational tool devised to perform an exhaustive computation of coarse dynamics (e.g., steady states) across all possible parameter

Table 1 | Column 1: Input values to node A

Input value	θ_{BA}	θ_{CA}	θ_{DA}
$I1 = l_{AB}l_{AC}l_{AD}$	$I1<\theta_{BA}$	$I1<\theta_{CA}$	$I1<\theta_{DA}$
$I2 = u_{AB}l_{AC}l_{AD}$	$I2>\theta_{BA}$	$I2>\theta_{CA}$	$I2<\theta_{DA}$
$I3 = l_{AB}u_{AC}l_{AD}$	$I3>\theta_{BA}$	$I3>\theta_{CA}$	$I3<\theta_{DA}$
$I4 = l_{AB}l_{AC}u_{AD}$	$I4>\theta_{BA}$	$I4>\theta_{CA}$	$I4>\theta_{DA}$
$I5 = u_{AB}u_{AC}l_{AD}$	$I5>\theta_{BA}$	$I5>\theta_{CA}$	$I5<\theta_{DA}$
$I6 = u_{AB}l_{AC}u_{AD}$	$I6>\theta_{BA}$	$I6>\theta_{CA}$	$I6>\theta_{DA}$
$I7 = l_{AB}u_{AC}u_{AD}$	$I7>\theta_{BA}$	$I7>\theta_{CA}$	$I7>\theta_{DA}$
$I8 = u_{AB}u_{AC}u_{AD}$	$I8>\theta_{BA}$	$I8>\theta_{CA}$	$I8>\theta_{DA}$

Columns 2–4: A choice of input value relationships to output thresholds. As discussed in the text, this table represents an example of two DSGRN parameters for node A.

Table 2 | Column 1: The input value to node A

Input values	θ_{BA}	θ_{CA}	θ_{DA}
$I1 = l_{AB}l_{AC}l_{AD}$	$I1<\theta_{BA}$	$I1<\theta_{CA}$	$I1<\theta_{DA}$
$I2 = u_{AB}l_{AC}l_{AD}$	$I2<\theta_{BA}$	$I2<\theta_{CA}$	$I2<\theta_{DA}$
$I3 = l_{AB}u_{AC}l_{AD}$	$I3<\theta_{BA}$	$I3<\theta_{CA}$	$I3<\theta_{DA}$
$I4 = l_{AB}l_{AC}u_{AD}$	$I4>\theta_{BA}$	$I4>\theta_{CA}$	$I4>\theta_{DA}$
$I5 = u_{AB}u_{AC}l_{AD}$	$I5<\theta_{BA}$	$I5<\theta_{CA}$	$I5<\theta_{DA}$
$I6 = u_{AB}l_{AC}u_{AD}$	$I6>\theta_{BA}$	$I6>\theta_{CA}$	$I6>\theta_{DA}$
$I7 = l_{AB}u_{AC}u_{AD}$	$I7>\theta_{BA}$	$I7>\theta_{CA}$	$I7>\theta_{DA}$
$I8 = u_{AB}u_{AC}u_{AD}$	$I8>\theta_{BA}$	$I8>\theta_{CA}$	$I8>\theta_{DA}$

Columns 2–4: A choice of input value relationships to output thresholds. As discussed in the text, this table represents an example of six DSGRN SB parameters for node A

values of a switching system[21]. The switching system for the TTr is given by four equations, one for each node. The equation for node A is given; the equations for the other nodes are analogous.

$$\frac{dA}{dt} = \sum_{X\in\{B,C,D\}} H_\infty^-(A, X, l_{AX}, u_{AX}, \theta_{AX}) - k_A{}^*A \tag{4}$$

$$H_\infty^-(Y, X, l_{YX}, u_{YX}, \theta_{YX}) = \begin{cases} u_{YX}, X < \theta_{YX} \\ l_{YX}, X > \theta_{YX} \end{cases} \tag{5}$$

Notice that $H_\infty^- = (u_{YX} - l_{YX}) \lim_{n\to\infty} \frac{1}{1+(X^n/\theta_{YX}^n)} + l_{YX}$, which permits a mapping from RACIPE parameters to DSGRN parameter regions (see[21] for details). We refer to $l_{YX}, u_{YX}, \theta_{YX}$ as the lower, upper, and threshold values of the edge $X \to Y$.

The parameter regions defined by DSGRN are given by collections of inequalities derived from the topology of the TTr, one for each of A, B, C, and D. Each node has three input edges, and therefore has eight potential input values (example shown for node A in the first column of Table 1). These input values to A are interleaved with the thresholds θ_{XA} of A's output edges to form a DSGRN parameter region for the A node. An example set of DSGRN parameter inequalities for node A is given in the 2nd-4th columns of Table 1.

The table above implicitly defines $\theta_{BA}<\theta_{DA}$ and $\theta_{CA}<\theta_{DA}$; however, the relationship of θ_{BA}, θ_{CA} remains an open choice, and therefore the table represents two DSGRN parameter regions. The dynamics and, thus, the different possible steady-state values for each node are determined by a choice of DSGRN parameter[20]. For the TTr, there are 3 in-edges and 3 out-edges from every node, resulting in 4242 parameter regions for each node. Each node independently may be associated with any one of these inequalities, resulting in 4242^4 DSGRN parameter regions, an incomputable number. Instead of exhaustive computations, we use both stochastic sampling and a principled restriction of the number of DSGRN parameter regions.

Stochastic simulations

As previously stated, the number of DSGRN parameter regions for TTr makes exhaustive computing infeasible. We randomly sampled four sets of 10,000 DSGRN parameters, for a total of 40,000 parameters. For each sample group, we used the DSGRN software (https://github.com/marciogameiro/DSGRN) to calculate the discrete dynamics of each parameter, and hence the classification of its monostability, bistability or other multistability.

Strict monotone Boolean parameters

Modelling using monotone Boolean functions has a long history[58,59]. DSGRN parameters are readily described as multilevel Boolean functions[60], which have a special subset of monotone Boolean functions. We restrict our attention to these DSGRN parameter regions, which we call strict monotone Boolean (SB) parameters. The set of SB parameters are all DSGRN parameter regions (i.e., they respect the partial order in Table 2) such that an input value *Ik* is either less than or equal to all the output thresholds of node A. An example SB parameter is given in Table 2, where again, less than relationships are highlighted in red. Notice that in every row (i.e., each input value) the signs are either all ">" or all "<", this is the condition to be an SB parameter. We note that there are additional algebraic constraints on DSGRN parameters. Specifically, the input values (i.e., the lower and upper values) into a node are evaluated as a sum of products, see[20] for more details.

In a SB parameter, there are no input values between any two thresholds, and therefore, the thresholds may occur in any of the six possible orders. Therefore, a SB parameter table always represents six DSGRN parameter regions. Given the small size of this collection of parameters (6561) compared to all parameters, the high correlation between the results from RACIPE sampling, SB parameters, and sampling of all DSGRN parameters exhibited in Fig. 3B, D is surprising. We are currently an seeking explanation of this phenomenon.

Data availability

The codes used in manuscript to generate all simulation data are available here: https://github.com/The-Aviator-Frames/Toggle-Tetrahedron and https://github.com/Eandreas1857/Tetrahedron.

Received: 15 March 2024; Accepted: 1 September 2024;
Published online: 24 October 2024

References

1. Laurent, M. & Kellershohn, N. Multistability: A major means of differentiation and evolution in biological systems. *Trends Biochem Sci.* **24**, 418–422 (1999).
2. Guantes, R. & Poyatos, J. F. Multistable decision switches for flexible control of epigenetic differentiation. *PLoS Comput Biol.* **4**, e1000235 (2008).
3. Zhou, J. X. & Huang, S. Understanding gene circuits at cell-fate branch points for rational cell reprogramming. *Trends Genet.* **27**, 55–62 (2011).
4. Gardner, T. S., Cantor, C. R. & Collins, J. J. Construction of a genetic toggle switch in Escherichia coli. *Nature* **403**, 339–342 (2000).
5. Dupage, M. & Bluestone, J. A. Harnessing the plasticity of CD4+ T cells to treat immune-mediated disease. *Nat. Rev. Immunol. 2016* **16**, 149–163 (2016).
6. Fang, D. & Zhu, J. Dynamic balance between master transcription factors determines the fates and functions of CD4 T cell and innate lymphoid cell subsets. *J. Exp. Med.* **214**, 1861–1876 (2017).
7. Duddu, A. S., Sahoo, S., Hati, S., Jhunjhunwala, S. & Jolly, M. K. Multistability in cellular differentiation enabled by a network of three

mutually repressing master regulators. *J. R. Soc. Interface* **17**, 20200631 (2020).
8. Tortola, L. et al. High-Dimensional T Helper Cell Profiling Reveals a Broad Diversity of Stably Committed Effector States and Uncovers Interlineage Relationships. *Immunity* **53**, 597–613.e6 (2020).
9. Zhou, L. et al. TGF-β-induced Foxp3 inhibits TH17 cell differentiation by antagonizing RORγt function. *Nature* **453**, 236–240 (2008).
10. Mantel, P. Y. et al. GATA3-Driven Th2 Responses Inhibit TGF-β1–Induced FOXP3 Expression and the Formation of Regulatory T Cells. *PLoS Biol.* **5**, e329 (2007).
11. Lazarevic, V. et al. T-bet represses TH17 differentiation by preventing Runx1-mediated activation of the gene encoding RORγt. *Nat. Immunol. 2010* **12**, 96–104 (2010).
12. Hong, T., Xing, J., Li, L. & Tyson, J. J. A Mathematical Model for the Reciprocal Differentiation of T Helper 17 Cells and Induced Regulatory T Cells. *PLoS Comput Biol.* **7**, e1002122 (2011).
13. Hansmann, L. et al. Dominant Th2 differentiation of human regulatory T cells upon loss of FOXP3 expression. *J. Immunol.* **188**, 1275–1282 (2012).
14. Levine, A. G. et al. Stability and function of regulatory T cells expressing the transcription factor T-bet. *Nature* **546**, 421–425 (2017).
15. Höllbacher, B. et al. Transcriptomic Profiling of Human Effector and Regulatory T Cell Subsets Identifies Predictive Population Signatures. *Immunohorizons* **4**, 585–596 (2020).
16. Kanno, T. et al. Characterization of proteogenomic signatures of differentiation of CD4. T cell subsets. *DNA Res.* **30**, dsac54 (2023).
17. Duddu, A. S., Majumdar, S. S., Sahoo, S., Jhunjhunwala, S. & Jolly, M. K. Emergent dynamics of a three-node regulatory network explain phenotypic switching and heterogeneity: a case study of Th1/Th2/Th17 cell differentiation. *Mol. Biol. Cell* **33**, ar46 (2022).
18. Huang, B. et al. Interrogating the Topological Robustness of Gene Regulatory Circuits. *PLoS Comput Biol.* **13**, e1005456 (2017).
19. Gedeon, T. Multi-parameter exploration of dynamics of regulatory networks. *Biosystems* **190**, 104113 (2020).
20. Cummins, B., Gedeon, T., Harker, S., Mischaikow, K. & Mok, K. Combinatorial representation of parameter space for switching networks. *SIAM J. Appl Dyn. Syst.* **15**, 2176–2212 (2016).
21. Hari, K. et al. Assessing biological network dynamics: comparing numerical simulations with analytical decomposition of parameter space. *NPJ Syst. Biol.Appl* **9**, 29 (2023).
22. Jolly, M. K. et al. Interconnected feedback loops among ESRP1, HAS2, and CD44 regulate epithelial-mesenchymal plasticity in cancer. *APL Bioeng.* **2**, 31908 (2018).
23. Bending, D. et al. A temporally dynamic Foxp3 autoregulatory transcriptional circuit controls the effector Treg programme. *EMBO J.* **37**, 99013 (2018).
24. Hagberg A. A., Schult D. A., Swart P. J. 2008 Exploring Network Structure, Dynamics, and Function using NetworkX. In *Proceedings of the 7th Python in Science Conference* (eds G. Varoquaux, T. Vaught, J. Millman), pp. 11–15. Pasadena, CA USA.
25. Hari, K. et al. Identifying inhibitors of epithelial-mesenchymal plasticity using a network topology based approach. *NPJ Syst. Biol. Appl* **6**, 15 (2020).
26. Hari, K., Ullanat, V., Balasubramanian, A., Gopalan, A. & Jolly, M. K. Landscape of epithelial mesenchymal plasticity as an emergent property of coordinated teams in regulatory networks. *Elife* **11**, e76535 (2022).
27. Chauhan, L., Ram, U., Hari, K. & Jolly, M. K. Topological signatures in regulatory network enable phenotypic heterogeneity in small cell lung cancer. *Elife* **10**, e64522 (2021).
28. Harlapur, P., Duddu, A. S., Hari, K., Kulkarni, P. & Jolly, M. K. Functional Resilience of Mutually Repressing Motifs Embedded in Larger Networks. *Biomolecules* **12**, 1842 (2022).
29. Zhu, R., del Rio-Salgado, J. M., Garcia-Ojalvo, J. & Elowitz, M. B. Synthetic multistability in mammalian cells. *Science* **375**, eabg9765 (2022).
30. Santos-Moreno, J., Tasiudi, E., Stelling, J. & Schaerli, Y. Multistable and dynamic CRISPRi-based synthetic circuits. *Nat. Comm.* **11**, 2746 (2020).
31. Yang, Y., Nemhauser, J. L. & Klavins, E. Synthetic Bistability and Differentiation in Yeast. *ACS Synth. Biol.* **8**, 929–936 (2019).
32. Wu, F., Su, R.-Q., Lai, Y.-C. & Wang, X. Engineering of a synthetic quadrastable gene network to approach Waddington landscape and cell fate determination. *Elife* **6**, 23702 (2017).
33. Jolly, M. K. et al. Operating principles of Notch-Delta-Jagged module of cell-cell communication. *New J. Phys.* **17**, 055021 (2015).
34. Pfeuty, B. Multistability and transitions between spatiotemporal patterns through versatile Notch-Hes signaling. *J. Theor. Biol.* **539**, 111060 (2022).
35. Bocci, F., Jia, D., Nie, Q., Jolly, M. K. & Onuchic, J. Theoretical and computational tools to model multistable gene regulatory networks. *Rep. Prog. Phys.* **86**, 106601 (2023).
36. Tian, T. & Burrage, K. Stochastic models for regulatory networks of the genetic toggle switch. *Proc. Natl Acad. Sci. USA* **103**, 8372–8377 (2006).
37. Jaruszewicz, J. & Lipniacki, T. Toggle switch: Noise determines the winning gene. *Phys. Biol.* **10**, 035007 (2013).
38. Strasser, M., Theis, F. J. & Marr, C. Stability and Multiattractor Dynamics of a Toggle Switch Based on a Two-Stage Model of Stochastic Gene Expression. *Biophys. J.* **102**, 19 (2012).
39. Lu, M., Onuchic, J. & Ben-Jacob, E. Construction of an Effective Landscape for Multistate Genetic Switches. *Phys. Rev. Lett.* **113**, 078102 (2014).
40. Tripathi, S., Kessler, D. A. & Levine, H. Biological Networks Regulating Cell Fate Choice Are Minimally Frustrated. *Phys. Rev. Lett.* **125**, 088101 (2020).
41. Huang, S., Guo, Y. P., May, G. & Enver, T. Bifurcation dynamics in lineage-commitment in bipotent progenitor cells. *Dev. Biol.* **305**, 695–713 (2007).
42. Peine, M. et al. Stable T-bet+GATA-3+ Th1/Th2 Hybrid Cells Arise In Vivo, Can Develop Directly from Naive Precursors, and Limit Immunopathologic Inflammation. *PLoS Biol.* **11**, e1001633 (2013).
43. Yang, B. H. et al. Foxp3(+) T cells expressing RORγt represent a stable regulatory T-cell effector lineage with enhanced suppressive capacity during intestinal inflammation. *Mucosal. Immunol.* **9**, 444–457 (2016).
44. Burt, P. et al. Dissecting the dynamic transcriptional landscape of early T helper cell differentiation into Th1, Th2, and Th1/2 hybrid cells. *Front Immunol.* **13**, 928018 (2022).
45. Magni, S. et al. Inferring upstream regulatory genes of FOXP3 in human regulatory T cells from time-series transcriptomic data. *npj Syst. Biol. Appl. 2024 10, 59 (2024)* **10**, 59 (2024).
46. Ma, S., Ming, Y., Wu, J. & Cui, G. Cellular metabolism regulates the differentiation and function of T-cell subsets. *Cell. Mol. Immunol. 2024* **21**, 419–435 (2024).
47. Hegazy, A. N. et al. Plasticity and lineage commitment of individual TH1 cells are determined by stable T-bet expression quantities. *Sci. Adv.* **10**, 2693 (2024).
48. Puniya, B. L. et al. A mechanistic computational model reveals that plasticity of CD4+ T cell differentiation is a function of cytokine composition and dosage. *Front Physiol.* **9**, 878 (2018).
49. Hong, T., Oguz, C. & Tyson, J. J. A Mathematical Framework for Understanding Four-Dimensional Heterogeneous Differentiation of CD4+ T Cells. *Bull. Math. Biol.* **77**, 1046–1064 (2015).
50. Johnston, R. J. et al. Bcl6 and Blimp-1 are reciprocal and antagonistic regulators of T follicular helper cell differentiation. *Science* **325**, 1006–1010 (2009).

51. Kusam, S., Toney, L. M., Sato, H. & Dent, A. L. Inhibition of Th2 differentiation and GATA-3 expression by BCL-6. *J. Immunol.* **170**, 2435–2441 (2003).
52. Cimmino, L. et al. Blimp-1 attenuates Th1 differentiation by repression of ifng, tbx21, and bcl6 gene expression. *J. Immunol.* **181**, 2338–2347 (2008).
53. Garg, G. et al. Blimp1 Prevents Methylation of Foxp3 and Loss of Regulatory T Cell Identity at Sites of Inflammation. *Cell Rep.* **26**, 1854–1868.e5 (2019).
54. Ogawa, C. et al. Blimp-1 Functions as a Molecular Switch to Prevent Inflammatory Activity in Foxp3+RORγt+ Regulatory T Cells. *Cell Rep.* **25**, 19 (2018).
55. Brunner P., Kiwitz L., Li L., Thurley K. Diffusion-limited cytokine signaling in T cell populations. *iScience* **27**. https://doi.org/10.1016/j.isci.2024.110134 (2024).
56. Font-Clos, F., Zapperi, S. & La Porta, C. A. M. Topography of epithelial–mesenchymal plasticity. *Proc. Natl Acad. Sci. USA* **115**, 5902–5907 (2018).
57. Cordella, L. P., Foggia, P., Sansone, C. & Vento, M. A (sub)graph isomorphism algorithm for matching large graphs. *IEEE Trans. Pattern Anal. Mach. Intell.* **26**, 1367–1372 (2004).
58. Abou-Jaoudé, W. & Monteiro, P. T. On logical bifurcation diagrams. *J. Theor. Biol.* **466**, 39–63 (2019).
59. Thomas, R. Boolean formalization of genetic control circuits. *J. Theor. Biol.* **42**, 563–585 (1973).
60. Crawford-Kahrl, P., Cummins, B. & Gedeon, T. Joint realizability of monotone Boolean functions. *Theor. Comput Sci.* **922**, 447–474 (2022).
61. Schneider, A., Hommel, G. & Blettner, M. Linear regression analysis: part 14 of a series on evaluation of scientific publications. *Dtsch Arztebl Int* **107**, 776–782 (2010).

Acknowledgements

T.G., B.C. and E.A. were partially supported by NSF grant DMS-1839299 and NIH 5R01GM126555-01. A.S.D., H.B.V. and K.H. were supported by Prime Minister's Research Fellowship, Government of India. M.K.J. was supported by Ramanujan Fellowship (SB/S2/RJN-049/2018), Science and Engineering Board, Government of India. M.K.J. was also supported by Param Hansa Philanthropies.

Author contributions

M.K.J., B.C. and T.G. designed and supervised the research. A.S.D., E.A., H.B.V., K.G., V.R.S. and K.H. conducted simulations and/or transcriptomic data analysis. A.S.D., K.H., S.J., B.C., T.G. and M.K.J. analysed data. All authors contributed to writing the manuscript.

Competing interests

MKJ serves as Editor-in-Chief of this journal and had no role in the peer-review or decision to publish this manuscript. MKJ declares no financial competing interests. All other authors declare no financial or non-financial competing interests.

Additional information

Supplementary information The online version contains supplementary material available at https://doi.org/10.1038/s41540-024-00433-6.

Correspondence and requests for materials should be addressed to Breschine Cummins, Tomas Gedeon or Mohit Kumar Jolly.